Accepted Manuscript

Studies of anticancer activity in vitro and in vivo of iridium(III) polypyridyl complexes-loaded liposomes as drug delivery system

Wen-Yao Zhang, Fan Du, Miao He, Lan Bai, Yi-Ying Gu, Lin-Lin Yang, Yun-Jun Liu

PII: S0223-5234(19)30525-2

DOI: https://doi.org/10.1016/j.ejmech.2019.06.009

Reference: EJMECH 11412

To appear in: *European Journal of Medicinal Chemistry*

Received Date: 3 June 2019

Accepted Date: 3 June 2019

Please cite this article as: W.-Y. Zhang, F. Du, M. He, L. Bai, Y.-Y. Gu, L.-L. Yang, Y.-J. Liu, Studies of anticancer activity in vitro and in vivo of iridium(III) polypyridyl complexes-loaded liposomes as drug delivery system, *European Journal of Medicinal Chemistry* (2019), doi: https://doi.org/10.1016/j.ejmech.2019.06.009.

Graphic abstract

Two iridium(III) complexes $[Ir(ppy)_2(HPIP)](PF_6)$ (**Ir-1**) and $[Ir(ppy)_2(BHPIP)](PF_6)$ (**Ir-2**) were synthesized and characterized. The complexes **Ir-1** and **Ir-2** were encapsulated in liposomes **Ir-1-Lipo** and **Ir-2-Lipo**. The anticancer activity of the complexes and liposomes was investigated by apoptosis, comet assay, ROS, mitochondrial membrane potential, release of cytochrome c, tubules and western blot analysis and in vivo antitumor activity.

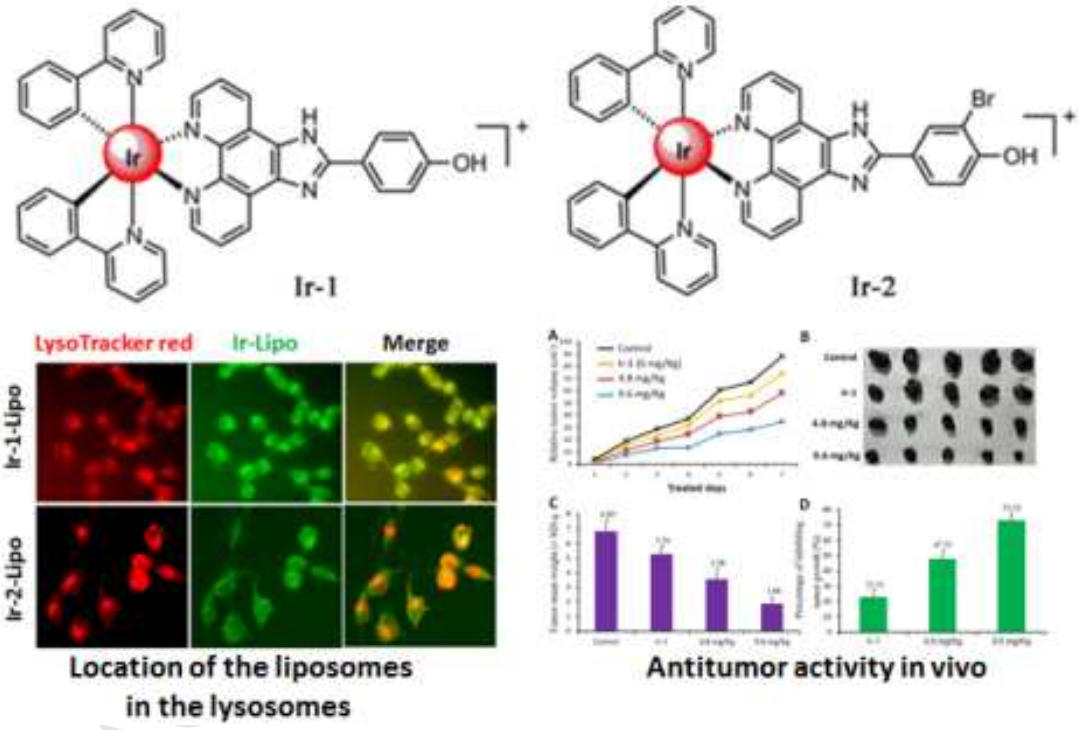

Submitted to Eur J Med Chem.

Studies of anticancer activity in vitro and in vivo of iridium(III) polypyridyl complexes-loaded liposomes as drug delivery system

Wen-Yao Zhang[a], Fan Du[a], Miao He[a], Lan Bai[a], Yi-Ying Gu[a], Lin-Lin Yang[b,*], Yun-Jun Liu[a,c*]

[a]*School of Pharmacy, Guangdong Pharmaceutical University, Guangzhou, 510006, P.R. China*

[b]*Department of Pediatrics, Guangdong Women and Children Hospital, Guangzhou 510000, P.R. China*

[c]*Guangdong Engineering Research Center for lead compounds & Drug Discovery, Guangzhou, 510006, P.R. China*

*Corresponding author. *E-mail address:* fy_yanglinlin@126.com (L.L. Yang);

lyjche@gdpu.edu.cn (Y.J. Liu).

Abstract: Two iridium(III) polypyridyl complexes $[Ir(ppy)_2(HPIP)](PF_6)$ (**Ir-1**), $[Ir(ppy)_2(BHPIP)](PF_6)$ **(Ir-2)** and their liposomes **Ir-1-LIpo** and **Ir-2-Lipo** were synthesized and characterized by elemental analysis, IR, ^{1}H NMR and ^{13}C NMR. The anticancer activity in vitro and in vivo was evaluated. The cytotoxic activity in vitro of the complexes and their liposomes **Ir-1-Lipo** and **Ir-2-Lipo** against cancer cells was investigated by MTT methods. **Ir-1** and **Ir-2** show no cytotoxic activity, while **Ir-1-Lipo** and **Ir-2-Lipo** exhibit high cytotoxic effect. The IC_{50} values range from 5.2 ± 0.8 to 22.3 ± 1.8 μM. The apoptosis, reactive oxygen species, the change of mitochondrial membrane potential, intracellular Ca^{2+} levels and a release of cytochrome c were investigated. The effect of **Ir-1-Lipo** and **Ir-2-Lipo** on tubules was also explored. In the C57BL/6 mice model, **Ir-1** only displays a tumor inhibitory rate of 23.21%, while **lr-1-Lipo** exhibits satisfactory in vivo antitumor efficacy with tumor inhibitory rate of 72.55%. This study demonstrates that complexes encapsulated in liposomes induce apoptosis in B16 through ROS-mediated lysosomal-mitochondria dysfunction, inhibition of polymerization of microtubules and induce cell cycle arrest at S phase.

Keywords: Iridium(III) polypyridyl complexes; Liposomes; Cytotoxicity in vitro and in vivo assays; Microtubules; ROS.

1. Introduction

Cancer remains one of the most challenging and dangerous health burden for human beings worldwide. Although, in the past decades, great efforts have been attempted to overcome cancer, it is still challenging to defeat the disease [1]. The main cause of cancer-related death is not the tumor itself but the metastasis from the tumor [2]. Chemotherapy is the commonly applied approach for cancer management, but the toxic and side effects make chemotherapy become troublesome [3]. With the successful clinical application of cisplatin, the therapeutic value of metal-based drugs has long been established [4]. However, this platinum-based drug has several adverse side effects, such as renal toxicity, myelosuppression, nausea, vomiting, and cytotoxicity, which frequently limit its use in the clinic [5,6]. In order to overcome these limitations, more attention has been paid to find anti-cancer activities in other metal complexes as alternatives of cisplatin. Among metal complexes, organometallic iridium complexes have recently emerged as promising alternatives and are expected to overcome the limitations of platinum-based drugs [7-9]. It has been reported that iridium(III) complexes generate reactive oxygen species to induce apoptosis by acting on mitochondria and exert anticancer effects through interaction with DNA [10-12].

In order to overcome the disadvantages of metal complexes, there is an urgent need to engineer multifunctional transfer systems to improve the biochemical characteristics of iridium(III) complexes. In the past decades, nanocarrier-based drug delivery systems (DDS) have gained increasing attention. It has been widely accepted that nanoparticles with a diameter of 20 to 200 nm can passively target solid tumor tissues [13,14]. Considering the passive targeting ability through enhancing

permeability and retention (EPR) effects, the metal complexes tend to be loaded into nanoparticles [15], micelles [16-18], liposomes [19], and sorts of nanodispersions. And it is very important to choose the right materials or the nanocarriers. Among various carriers, liposomes with similar properties to biofilms represent the most acceptable form of parenteral delivery system due to their high biocompatibility and safety [20]. Surface conjugation by polyethylene (glycol) (PEG) can improve the liposome's systemic circulation [21,22]. And the nano-sized and hydrophilic layer of PEG will prolong liposome blood circulation. As far as we know, the studies of anticancer activity of iridium(III) complexes encapsulated in liposomes has been paid less attention so far.

To obtain more insight of iridium (III) complexes and their liposomes on anticancer activity and mechanism, in this report, we synthesized two new iridium(III) complexes $[Ir(ppy)_2(HPIP)](PF_6)$ (ppy = 2-phenylpyridine, HPIP = 2-(4-hydroxy)phenylimidazo[4,5-*f*][1,10]phenanthroline, **Ir-1**) and $[Ir(ppy)_2(BHPIP)](PF_6)$ (BHPIP = 2-(3-bromo-4-hydroxy)phenylimidazo[4,5-*f*][1,10]phenanthroline, **Ir-2**, Scheme 1) and characterized by elemental analysis, IR, ESI-MS, ^{1}H NMR and ^{13}C NMR. To improve the pharmacokinetics and increase the anticancer effect of complexes, **Ir-1** and **Ir-2**-loaded PEGylated liposomes (**Ir-1-Lipo**, **Ir-2-Lipo**) were prepared based on reverse-phase-evaporation method. The liposomes **Ir-1-Lipo** and **Ir-2-Lipo** were characterized by particle size, drug entrapment and morphology and release in vitro. The cellular trafficking mechanism, cytotoxicity， reactive oxygen species and

apoptotic effect of **Ir-1-Lipo**, **Ir-2-Lipo** on B16 cells were investigated in detail. Finally, the antitumor efficacy in vivo of **Ir-1** and **Ir-1-Lipo** was evaluated in B16 tumor-bearing mice.

2. Results and discussion

*2.1. Synthesis and characterization of complexes **Ir-1**, **Ir-2** and liposomes **Ir-1-Lipo** and **Ir-2-Lipo***

The ligands HPIP and BHPIP were obtained by reacting 1,10-phenanthroline-5,6-dione and ammonium acetate with 4-hydroxybenzaldehyde or 3-bromo-4-hydroxybenzaldehyde in glacial acetic acid solvent. The complexes $[Ir(ppy)_2(HPIP)](PF_6)$ (**Ir-1**) and $[Ir(ppy)_2(BHPIP)](PF_6)$ (**Ir-2**) were synthesized by the direct reaction of HPIP or BHPIP and precursor complex cis-$[Ir(ppy)_2Cl]_2$ in a mixture of dichloromethane and methanol. The synthesized complexes **Ir-1** and **Ir-2** were characterized by elemental analysis, ESI-MS, IR, ^{1}H NMR and ^{13}C NMR. The liposomes were prepared by reverse-phase-evaporation method. The mole ratio of phospholipid/cholesterol and drug/lipid at 3:1 and 1:30 was used to produce stable liposomes and achieve high drug loading. The average particle size of **Ir-1-Lipo** and **Ir-2-Lipo** is 123.6 nm and 113.5 nm (Fig. S1, supporting information). The ζ potentials of **Ir-1-Lipo** and **Ir-2-Lipo** are −35.60 ± 1.26 mV and −13.23 ± 1.94 mV, respectively. When the absolute value of zeta potential exceeded 30 mV, the liposomes were regarded as highly stable, while the zeta potential in the range of 10-20 mV indicated the liposomes were relatively stable [23]. These data indicate that

the liposomes are stable. The morphology of the particle was observed via TEM imaging. The particles are perfectly spherical in shape and distributed fairly uniform in the copper grid (Fig. S2, supporting information), which also shows that liposomes have a stable morphology. Therefore, all these results identified that the **Ir-1** and **Ir-2** prodrug can be encapsulated in stable and well-defined liposomes.

The UV-Vis spectra of 10 µM of **Ir-1**, **Ir-2**, **Ir-1-Lipo** and **Ir-2-Lipo** in PBS solution are shown in Fig. S3 (supporting information). The maximum absorbance of **Ir-1**, **Ir-2**, **Ir-1-Lipo** and **Ir-2-Lipo** appears at 208, 204, 202 and 205 nm, respectively. The complexes (1.1 µM) and their liposomes (1.1 µM) can emit luminescence in PBS solution at ambient temperature (Fig. S4, supporting information), with a maximum appearing at 499, 500, 500 and 499 nm for **Ir-1**, **Ir-2**, **Ir-1-Lipo** and **Ir-2-Lipo**, respectively.

2.2. In vitro drug release studies

The in vitro drug release was performed in phosphate buffered saline (pH 7.4) containing 1% SDS (w/v) by dialysis method. The release profiles of **Ir-1** from **Ir-1-Lipo** and **Ir-2** from **Ir-2-Lipo** are shown in Fig. 1. The results clearly revealed that the encapsulated **Ir-1** and **Ir-2** released in a sustained manner without any sign of burst release. Lack of any burst release indicates that all of the drug encapsulated in the lipid bilayer and not present in the outer surface. Fig. 1 shows that **Ir-1** released in a fast rate compared to **Ir-2**. The accumulative release of **Ir-1-Lipo** was up to 18.8% within 48 h, while **Ir-2** released from **Ir-2-Lipo** was merely 13.8%. A controlled

release of drug from the nanocarrier system might be beneficial for the cancer treatment as it will provide a constant exposure of the anticancer drug to the cancer cells. In addition, the encapsulation efficiency (EE(%)) is 83.0% for **Ir-1-Lipo** and 70.0% for **Ir-2-Lipo**, respectively.

2.3. Cytotoxicity in vitro assays

The in vitro antiproliferative activities of **Ir-1**, **Ir-2**, **Ir-1-Lipo** and **Ir-2-Lipo** toward MCF-7, HeLa, B16, SGC-7901, A549, BEL-7402 and normal LO2 cell lines were investigated after 48 h exposure period using the MTT assays. The anti-tumor proliferative effects induced by the two complexes with subtle changes in chemical structure are also surprisingly similar. As shown in Table 1, the growth inhibition concentration (IC_{50}) values of 50% of the tumor cells obtained by **Ir-1** and **Ir-2** were both greater than 200 μM, and thus can be considered as inactive. However, it is surprising when complexes are encapsulated in liposomes, the anti-tumor activity is significantly improved. The IC_{50} values of **Ir-1-Lipo and Ir-2-Lipo** toward HeLa and B16 cells are 9.5 ± 0.9, 5.2 ± 0.8 μM and 6.2 ± 0.4 and 10.8 ± 1.5 μM, respectively. The cell viability of **Ir-1** (A, blue), **Ir-2** (B, blue), **Ir-1-Lipo** (A, red) and **Ir-2-Lipo** (B, red) against B16 cells is depicted in Fig. S5 (supporting information), obviously, all the liposomes exhibited a dose-dependent manner to inhibit the cell growth in B16. In summary, the ability of anti-tumor cell proliferation in vitro showed the following trends: **Ir-1-Lipo** > **Ir-1-Lipo** > **Ir-1** ≈ **Ir-2**. The liposomes **Ir-1-Lipo** and **Ir-2-Lipo** exhibit higher anticancer activity than complexes **Ir-1** and **Ir-2**, which may be caused

When complexes are encapsulated in liposomes to form a composite, they will be easier to enter into the cell to exert efficacy.

2.4. Location at the lysosomes and lysosomal permeabilization

Acidic organelle lysosomes are involved in a variety of physiological processes in cells, including protein breakdown, autophagy, induction of apoptosis, release of hydrolases and degradation of related receptors. It is worth noting that lysosomes in cancer cells are accompanied by an increase in the number and volume while the stability is decreasing. [24-26]. To study whether the complexes encapsulated liposomes target lysosomes, B16 cells were treated with 5.0 and 10.0 μM of **Ir-1-Lipo** and **Ir-2-Lipo** for 0.5 h, the cells were stained with LysoTracker red. It can be seen from Fig. 2 that the green fluorescence emitted by the liposomes **Ir-1-Lipo** and **Ir-2-Lipo** after entering the cell overlaps with the red fluorescence of the lysosome stained with LytoTracker red, and there is a perfect merge. This indicates that the liposomes **Ir-1-Lipo** and **Ir-2-Lipo** interact on the lysosomes of the cells.

Lysosome as a key target for anti-tumor therapy, the non-negligible factor is that lysosomal membrane permeabilization leads to protease infiltration into the cytoplasm triggering apoptosis pathway. The lysosomal metachromatic fluorescent dye AO, which represents a protonated oligomer (AOH^+) when the lysosomal membrane is stable, emits red fluorescence. However, when lysosomal membrane permeabilization occurs, the dye AO emits green fluorescence while represents in a deprotonated form [27]. As shown in Fig. S6 (supporting information), a number of obvious red

fluorescent points were observed in the control (a). However, after B16 cells were incubated with 5.0 and 10.0 μM of **Ir-1-Lipo** (b) and **Ir-2-Lipo** (c) for 24 h, the red fluorescence decreased and the green fluorescence increased, indicating that **Ir-1-Lipo** and **Ir-2-Lipo** can increase lysosomal membrane permeabilization.

2.5. Location of the liposomes at mitochondria and change of mitochondrial membrane potential

The cathepsin released after permeabilization of the lysosomal membrane can cause mitochondrial membrane permeation, which triggers the lysosomal-mitochondrial apoptosis pathway [28-30]. Mitochondria, the main energy supply site of cells, not only regulate cell growth and cell cycle, but also play an important role in cell signaling and apoptosis [31]. Increased mitochondrial membrane permeability will promote Ca^{2+} loaded in mitochondria, promote the release of a series of apoptotic factors such as cytochrome c, and induce apoptosis [32]. After B16 cells were treated with 5.0 and 10.0 μM of **Ir-1-Lipo** and **Ir-2-Lipo** for 1 h, the cells were stained with the dye MitoTracker Red to assess whether the liposomes target to the mitochondria. The red fluorescence emitted by the mitochondria stained by MitoTracker Red and the green fluorescence emitted by the liposomes **Ir-1-Lipo** and **Ir-2-Lipo** are clearly seen from Fig. 3. Interestingly, the two-color fluorescence can be perfectly superimposed, indicating that the liposomes **Ir-1-Lipo** and **Ir-2-Lipo** are targeted to the mitochondria.

Mitochondrial membrane potential is formed during mitochondrial respiratory

oxidation and is closely related to the cellular mitochondrial apoptosis pathway. Once the mitochondrial membrane potential is reduced, the cells will enter an irreversible process of apoptosis. Therefore, the mitochondrial membrane potential was investigated by using the fluorescent probe JC-1 on BI6 cells treated with the liposomes **Ir-1-Lipo** and **Ir-2-Lipo**. It is well known that JC-1 is a lipophilic cationic dye that selectively translocates to mitochondria and undergoes color changes with the changes in mitochondrial membrane potential (ΔΨm) [33]. In normal cells with a higher ΔΨm, JC-1 exists in the mitochondrial matrix in the form of a polymer (J-aggregates) and emits red fluorescence, and when it is in apoptotic cells, it exists in a monomeric form to emit green fluorescence. As shown in Fig. S7 (supporting information), the red fluorescence in most B16 cells (a) is converted to green fluorescence after 24 h of treatment with **Ir-1-Lipo** (b, 5 μM) and **Ir-2-Lipo** (c, 10 μM), indicating the loss of MMP. The depolarization ratio of mitochondria was obtained by analyzing the fluorescence intensity of green/red value of JC-1 by the ImageXpress Micro XLS system (Fig. S8, supporting information). The results showed that the liposomes **Ir-1-Lipo** and **Ir-2-Lipo** can decrease ΔΨm and cause mitochondrial dysfunction, which further mediates apoptosis of B16 cells through mitochondrial pathway.

2.6. Intracellular reactive oxygen species (ROS) detection

Mitochondria and lysosomes are the main sites of endogenous reactive oxygen species (ROS), in which mitochondria increase ROS levels by altering redox potential.

ROS, a class of single electron reduction products, is considered to be a key factor in apoptosis and inflammatory pathways [34]. The studies have shown that an increase in ROS levels promotes the opening of mitochondrial permeability transition pores and regulates the expression of some important pro-apoptotic proteins [35]. To gain insight into the anticancer mechanisms of these liposomes, the specific fluorescent probe DCFH-DA was used to investigate the changes in ROS levels in B16 cells. As shown in Fig. S9 (supporting information), incubation of B16 cells (a) with **Ir-1-Lipo** (b, 5 μM) and **Ir-2-Lipo** (c, 10 μM) markedly increased intracellular ROS levels as indicated by the increased levels of DCF fluorescence. The fluorescence intensity analysis by the ImageXpress Micro XLS system indicated that the green fluorescence intensity of DCF treated with **Ir-1-Lipo** and **Ir-2-Lipo** increased by 10.7 and 10.9 times, respectively, compared with the control group (Fig. S10, supporting information). The results demonstrate that liposomes **Ir-1-Lipo** and **Ir-2-Lipo** inhibit cancer cell proliferation by significantly increasing the level of endogenous ROS.

2.7. Determination of intracellular Ca^{2+} levels

Ca^{2+} is essential for normal life activities, especially during cell apoptosis and migration [36]. Subtle changes in Ca^{2+} distribution in subcellular structures are closely related to mitochondrial function and endogenous ROS levels [37-39]. The level of Ca^{2+} in mitochondria is significantly increased, which will promote the release of apoptotic factor cytochrome c and induce apoptosis of B16 cells. The results of intracellular Ca^{2+}, as reflected in changes in the fluorescence of the indicator dye

Fluo-3/AM, are shown in Fig. 4A. In the control (a), no obvious green fluorescent points were observed, indicating that the level of intracellular free Ca^{2+} is very low. However, B16 cells were incubated with **Ir-1-Lipo** (5.0 μM) and **Ir-2-Lipo** (10.0 μM) for 24 h, the green fluorescence intensity increases. To quantitatively analyze the Fluo-3 fluorescence intensity, it was found that the Ca^{2+} levels in cells treated with **Ir-1-Lipo** (5.0 μM) and **Ir-2-Lipo** (10.0 μM) increased by 8.1-fold and 6.0-fold compared with the control (Fig. 4B). The data demonstrate that liposomes can increase Ca^{2+} levels through the changes in mitochondrial dysfunction and ROS levels.

2.8. Detection of cytochrome c level

As a key protein in the mitochondria, cytochrome c has a non-negligible role in redox, energy metabolism, and apoptosis pathways. The changes in the endogenous ROS levels and mitochondrial damage will result in the release of cytochrome c, thereby inducing the formation of apoptotic bodies and accelerating the execution of apoptosis [40,41]. As is clear from Fig. 5A, the release of cytochrome c in B16 cells was significantly increased after the treatment of B16 cells with **Ir-1-Lipo** (5.0 μM) and **Ir-2-Lipo** (10.0 μM) for 24 h. The green fluorescence intensity was determined, as shown in Fig. 5B, it was found that the release of cytochrome c by liposome showed concentration tolerance, whereas the complexes **Ir-1** and **Ir-2** showed a slight effect on cytochrome c release.

2.9. Assay of apoptosis

It is well known that the infinite growth of cancer cells is closely related to the inhibition of apoptosis [42]. Therefore, the apoptosis was assayed by flow cytometry. The results of flow cytometry analysis of apoptosis induced by the complexes and liposomes treatment are shown in Fig. 6. In the control (a), the percentage in the early apoptosis is 0.96%. Simultaneously, it can be seen that after treatment of cells with **Ir-1** (b, 5.0 μM) and **Ir-2** (e, 10.0 μM) for 24 h, the percentage of early apoptosis of cells was 2.17% and 3.18%, respectively. This means that the complexes **Ir-1** and **Ir-2** have low effect on the apoptosis of B16 cells. However, B16 cells were exposed to 2.5 (c) and 5.0 μM (d) of **Ir-1-Lipo** or 5.0 (f) and 10.0 μM (g) of **Ir-2-Lipo** for 24 h, the percentages in the early apoptosis are 4.79% and 11.30%, 3.10% and 7.97%, respectively. The above results revealed a significant increase in early apoptosis of cells after treatment with liposomes **Ir-1-Lipo** and **Ir-2-Lipo** and a concomitant concentration tolerance.

2.10. DNA damage studies

DNA fragmentation in chromosomes is an important marker of apoptosis, and the degree of damage is explored by single cell gel electrophoresis experiments [43]. As shown in Fig. S11 (supporting information), a red fluorophore having no tailing phenomenon was observed in the control group (a), indicating that it stayed in the nuclear matrix due to the large molecular weight of the undamaged DNA in the cells. Interestingly, when B16 cells were treated with 5.0 μM **Ir-1-Lipo** (b) and 10.0 μM

Ir-2-Lipo (c) for 24 h, the comet-like fluorophore appeared in a fluorescence microscope. At the same time, when DNA damage in the nucleus is aggravated, it appears that the comet tail will become longer and the fluorescence will increase. The results show that the **Ir-1-Lipo** and **Ir-2-Lipo** can induce DNA fragmentation, providing further evidence of apoptosis.

2.11. Cell cycle arrest analysis

In the organism, a series of biological processes such as cell proliferation, growth, and differentiation receive regulation of the cell cycle [44]. The cell cycle-dependent protein kinases and their regulatory factors play an important role in the regulation of the cell cycle. Therefore, targeting the cancer cell proliferation cycle provides a new direction for the development of novel targeted drugs. The results of the periodic flow cytometry in Fig. S12 (supporting information) indicate that after treatment with 5.0 μM of **Ir-1-Lipo** and 10.0 μM of **Ir-2-Lipo** treated B16 cells for 24 h, we observed an increasing accumulation of cells in S phase and a decrease of cells in G0/G1 and G2/M phase, suggesting that **Ir-1-Lipo** and **Ir-2-Lipo** inhibit the cell growth in B16 cells at S phase, whereas **Ir-1** and **Ir-2** have no obvious effect on the cell cycle distribution. The cyclin-dependent kinase CDK2 is an important factor in ensuring that cells complete the G1 phase and enter the S phase. It is worth noting that overexpression of the protein CDK2 and cyclin A will accelerate the progression of the G1/S phase and induce tumorigenesis [45]. The molecular expression of the protein CDK2/cyclin A after B16 cells were treated with complexes and liposomes for

24 h is shown in Fig. 7A and 7B. The above results show that **Ir-1-Lipo** and **Ir-2-Lipo** can indeed induce S-phase cell cycle arrest.

2.13. In vitro inhibition of cell invasion

Metastasis of tumor cells is one of the main causes of cancer patients' difficulty in eradicating and dying. The destruction of cell cycle regulation mechanism is the root cause of cancer cell proliferation and migration. After demonstrating that liposomes can block cells in the S phase, the effect of liposomes on inhibiting cancer cell invasion is further explored. The invasion and migration ability of B16 cells after being treated by the complexes and liposomes was investigated by transwell chambers. The results of invasion inhibition are shown in Fig. S13 (supporting information), We can clearly observe that these liposomes have an excellent inhibitory effect on B16 cell invasion, and the inhibitory effect is enhanced with increasing concentration. In addition, B16 cells treated with liposome 2.5 (b) and 5.0 μM (c) **Ir-1-Lipo** and 5.0 (d) and 10.0 μM (e) **Ir-2-Lipo** were quantified to inhibit the number of invading cells for 24 h. It was found that the order of invasive inhibition was **Ir-1-Lipo** > **Ir-2-Lipo** >> **Ir-2** > **Ir-1** as shown in Fig. S14 (supporting information). Therefore, all the above results demonstrate that the liposomes **Ir-1-Lipo** and **Ir-2-Lipo** exhibit outstanding invasion inhibition ability to B16 cells.

2.14. Effects on the microtubule networks

Rearrangement of intracellular cytoskeletal proteins is a critical step leading to

tumor cell migration and invasion. Silk pseudopodia is not only the main structure of cytoskeleton formation, but also plays an important role in the initial stage of cancer cell invasion [46,47]. The cytoskeleton is a protein fiber network structure in eukaryotic cells, which can induce apoptosis when its morphology changes. To further understand whether liposomes inhibit the metastatic mechanism of cancer cells by targeting microtubules, microtubule morphology was studied by immunofluorescence staining. As shown in Fig. 8, in the control (a) and B16 cells were treated with 2.5 μM of **Ir-1-Lipo** (b) and 5.0 μM of **Ir-2-Lipo** (e), B16 cells were spread out with a well-organized microtubule network. However, after B16 cells were exposed to 5.0 μM of **Ir-1-Lipo** (c) and 10.0 μM of **Ir-2-Lipo** (f) for 24 h, it can be seen that the cells contract from the original shuttle to a round, polygonal, or irregular shape. The results indicated that the liposomes **Ir-1-Lipo** and **Ir-2-Lipo** triggered cell morphology collapse by inhibiting microtubule polymerization.

2.15. The mechanism studies of apoptosis

The mitochondrial apoptotic pathway is central to apoptosis during apoptosis [48], which is mainly regulated by proapoptotic proteins (Bax) and anti-apoptotic proteins (Bcl-2) in Bcl-2 family proteins [49,50]. Bcl-2 family proteins can induce mitochondrial membrane permeability and promote the release of apoptotic factor cytochrome c, which in turn leads to activation of caspase cascade and induction of apoptosis [51,52]. Therefore, the expression of apoptosis-related protein levels caused by liposome **Ir-1-Lipo** and **Ir-2-Lipo** was analyzed by Western blotting. After treated

with **Ir-1-lipo** and **Ir-2-lipo** for 24 h, the liposome could significantly increase the expression of protein Bax and strongly inhibit the expression of protein Bcl-2 as shown in Fig. 9A and 9B. The multiple apoptotic pathways of cells are closely related to the apoptosis-executing protein caspase-3 [53,54]. Therefore, the expression levels of protein caspase-3 and PARP in the mitochondrial apoptotic pathway are evaluated (Fig. 9A and 9B), and their expression levels are significantly up-regulated after being subjected to liposomes **Ir-1-Lipo** and **Ir-2-Lipo**. The results indicate that liposome-induced apoptosis of B16 cells could be carried out by the mitochondrial pathway.

*2.16. In vivo antitumor activity of **Ir-1** and **Ir-1-Lipo***

In order to further assess the anticancer effect of **Ir-1** and **Ir-1-Lipo** in vivo, antitumor efficacy study was performed in B16 cancer cell bearing tumor xenograft model. Mice were randomly divided into control and experimental groups. The mice were intraperitoneal injected different doses of **Ir-1-Lipo** (4.8 and 9.6 mg/kg) and **Ir-1** (6.0 mg/kg) every day for 7 days. As shown in Fig. 10, at the end of the treatment period, in the 4.8 mg/kg and 9.6 mg/kg of **Ir-1-Lipo** group, tumor volume was decreased 18.86% and 38.87% as compared with **Ir-1**-treated mice. Inhibition of high dose **Ir-1-Lipo** on tumor growth is more potent than those of low dose and **Ir-1**-treated group. Meanwhile, the tumor weight was also measured at the end of experiment. The tumor weight of **Ir-1-Lipo** (4.8 and 9.6 mg/kg) and **Ir-1**-treated group was 3.58 g, 1.88 g and 5.26 g, respectively. Inhibitory rate of tumor growth

induced by **Ir-1-Lipo** (4.8 and 9.6 mg/kg) treated group and **Ir-1**-treated group was 47.75%, 72.55% and 23.21%, respectively. This shows that the antitumor effect of **Ir-1-Lipo** is obviously concentration-dependent, and **Ir-1** was encapsulated in liposomes, the anticancer activity in vivo is enhanced.

3. Conclusions

In this study, we synthesized and characterized two new **Ir-1** and **Ir-2** complexes. The complexes show almost no anticancer activity against HeLa, A549, B16, MCF-7, SGC-7901, BEL-7402 and LO2 cells. Therefore, we have designed liposomes as biocompatible nanocarrier to deliver metal complexes. The particles exhibited a controlled release of drug in vitro. After encapsulated in liposomes, **Ir-1** and **Ir-2** showed high anticancer activity against B16 cells. **Ir-1-Lipo** and **Ir-2-Lipo** can cause apoptosis by increasing the level of intracellular reactive oxygen species and reducing mitochondrial membrane potential and further inducing mitochondrial dysfunction. On the other hand, **Ir-1-Lipo** and **Ir-2-Lipo** can target lysosomes and increase lysosomal permeabilization, target microtubules and inhibit the polymerization of microtubules. Additionally, **Ir-1-Lipo** and **Ir-2-Lipo** can cause DNA damage and inhibit the cell growth at S phase. In summary, **Ir-1-Lipo** and **Ir-2-Lipo** cause apoptosis through two major pathways (Fig. 11): (I) DNA damage and inhibiting polymerization of microtubules → cell cycle arrest → apoptosis; (II) Increase of intracellular ROS → lysosomal-mitochondrial dysfunction → release of cytochrome c and activation of caspase 3 → cleaved PARP → apoptosis. Most importantly,

Ir-1-Lipo exhibited a significantly superior anticancer effect on the tumor growth in vivo. This work is helpful for designing and synthesizing new iridium complexes as potent anticancer agents. In addition, the liposomal formulation can provide a promising platform for the delivery of metal-complex into tumor by enhancing therapeutic efficacy.

4. Experimental Section

4.1. Materials and methods

The purchased synthetic raw materials (4-hydroxybenzaldehyde, 3-bromo-4-hydroxybenzaldehyde, 2-phenylpyridine, 1,10-phenanthroline) and all reagents were used without further purification unless otherwise specified. Water obtained by purification from the Millipore Milli-Q system was used throughout the experiment. Fluorescent dye kits and related consumables are sourced from Beyotime Biotechnology. FBS and RPMI 1640 were purchased from Gibco company. The tumor cell lines SGC-7901, HeLa, BEL-7402, A549, B16, MCF-7 and normal LO2 cells were purchased from the American Type Culture Collection. Prior to each test, all complexes were dissolved in DMSO and the final concentration of DMSO was maintained at 1% (V/V). Elemental analysis of C, H, and N was performed by a PerkinElmer 240Q elemental analyzer. Electrospray ionization mass spectra were recorded by LCQ system (Finnigan MAT, USA) and the major peaks in the isotope distribution were represented by m/z values. ^{1}H NMR and ^{13}C NMR spectra were obtained by analysis on a Varian-500 spectrometer using DMSO-d_6 as a solvent at

room temperature.

4.2. Synthesis of complex

*4.2.1. Synthesis of [Ir(ppy)$_2$(HPIP)]PF$_6$ (**Ir-1**)*

A mixture of cis-[Ir(ppy)$_2$Cl]$_2$ (0.32 g, 0.3 mmol) [55] and HPIP (0.187 g, 0.6 mmol) [56] in a mixture of 42 mL of dichloromethane and methanol (V_{CH2Cl2}:VCH_3OH = 2:1) was refluxed under argon for 6 h to give a clear yellow solution. Upon cooling, a yellow precipitate was obtained by dropwise addition of saturated aqueous NH_4PF_6 solution with stirring at room temperature for 2 h. The crude product was purified by column chromatography on neutral alumina with a mixture of CH_2Cl_2/acetone (1:1, v/v) as eluent. The yellow band was collected. The solvent was removed under reduced pressure and a yellow powder was obtained. Yield: 74%. Anal. Calc for $C_{41}H_{28}N_6OIrPF_6$: C, 51.40; H, 2.95; N, 8.77. Found: C, 51.63; H, 2.81; N, 8.95. ^{1}HNMR: δ 9.12 (d, 2H, *J* = 8.5 Hz), 8.25 (d, 2H, *J* = 8.5 Hz), 8.12 (d, 2H, *J* = 8.5 Hz), 8.07 (d，2H, *J* = 5.0 Hz), 7.95 (d,4H, *J* = 5.0 Hz), 7.86 (t, 2H, *J* = 5.0 Hz), 7.50 (d, 2H, *J* = 6.5 Hz), 7.06 (t, 2H, *J* = 7.0 Hz), 7.01 (t, 2H, *J* = 7.0 Hz). ^{13}C NMR: 172.64, 167.01, 159.13, 150.78, 149.10, 147.48, 143.50, 138.71, 132.09, 131.31, 130.31, 128.38, 126.52, 125.11, 124.44, 123.89, 122.38, 120.01, 115.81. ESI-MS: m/z = 814 [M + 1].

*4.2.2. Synthesis of complex [Ir(ppy)$_2$(BHIP)]PF$_6$ (**Ir-2**)*

A mixture of cis-[Ir(ppy)$_2$Cl]$_2$ (0.32 g, 0.3 mmol) [54] and BHIP (0.23 g, 0.6

mmol) [57] in a mixture of 42 mL of dichloromethane and methanol (VCH_2Cl_2:VCH_3OH = 2:1) was refluxed under argon for 6 h to give a clear yellow solution. Upon cooling, a yellow precipitate was obtained by dropwise addition of saturated aqueous NH_4PF_6 solution with stirring at room temperature for 2 h. The crude product was purified by column chromatography on neutral alumina with a mixture of CH_2Cl_2/acetone (1:1, v/v) as eluent. The yellow band was collected. The solvent was removed under reduced pressure and a yellow powder was obtained. Yield: 72%. Anal. Calcd for $C_{41}H_{27}N_6OBrIrPF_6$: C, 47.49; H, 2.63; N, 8.11. Found: C, 47.61; H, 2.80; N, 8.02. ^{1}HNMR: δ 9.11 (d, 2H, *J* = 7.5 Hz), 8.43 (s, 1H,), 8.25 (d, 2H, *J* = 8.0 Hz), 8.13 (d, 1H, *J* = 8.0 Hz), 8.06 (d, 2H, *J* = 4.5 Hz), 7.95 (t, 4H, *J* = 7.5 Hz), 7.86 (t, 2H, *J* = 7.5 Hz), 7.50 (d, 2H, *J* = 6.0 Hz), 7.06 (t, 4H, *J* = 7.5 Hz), 6.98 (t, 4H, *J* = 8.0 Hz), 6.29 (d, 2H, *J* = 7.0 Hz), 3.55 (s, 1H). ^{13}C NMR: 172.28, 166.99, 155.98, 150.76, 149.08, 147.49, 144.09, 143.56, 138.69, 132.06, 131.30, 130.93, 130.29, 127.34, 126.53, 125.09, 124.57, 123.88, 122.37, 120.00, 116.85, 110.08. ESI-MS: m/z = 892 [M + 1].

4.3. Preparation of the liposomes

Ir-1-loaded PEGylated liposomes (**Ir-1-Lipo**) were prepared based on reverse-phase-evaporation method [58] as previously reported with minor modification. Briefly, **Ir-1**: PC-98T:CHO-HP (quality ratio 1:30:10) and PC-98T:DSPE-MPEG2000 (quality ratio 1:5%) were prepared and mixtures dissolving in chloroform and water (ratio of 3:1). Subsequently, the mixtures

sonicated to afford a white/brown emulsion-like mixture. The biphasic suspension was then transferred onto a rotary evaporator for gradual removal of the organic phase. Complete removal of organic solvents was achieved and added double distilled water at pH 7.4 for hydration, resultant crude liposome suspensions were diluted in double water (pH 7.4) distilled to provide required concentration of liposome concentration. Finally, sonication and centrifugation give the desired liposome. The preparation of **Ir-2-Lipo** is prepared in a manner identical to that described with **Ir-1-Lipo**.

4.4. Characterization of the liposomes

Ir-1-Lipo and **Ir-2-Lipo** were characterized by particle size, ζ potential and morphology. Particle size and ζ potential of liposomes were determined by Zetasizer Nano ZS (Malvern, UK). Morphology of liposomes was examined by transmission electron microscopy (TEM) (H-7650, Hitachi, Japan). The above samples were prepared by diluting them with appropriate amount of deionized water. TEM micrographs were acquired at the acceleration voltage of 100 kV.

4.5. In vitro drug release

The in vitro release of **Ir-1** and **Ir-2** from **Ir-1-Lipo** and **Ir-2-Lipo** was studied in phosphate buffered saline (PBS, pH 7.4) containing 1% SDS (w/v) by dialysis method. To conduct the release study, samples (200 µg) were filled in dialysis membrane (MWCO = 8-10 kDa) and the dialysis membrane was clipped and packed in a Falcon tube containing 200 ml of release medium. The tube as placed in shaking water bath

(Gongyi City Yuhua Instrument CO., LTD, China) and incubated at 37 ^{o}C (100 rpm). At predetermined intervals, 2 mL of release medium was withdrawn and replenished with 2 mL of fresh medium. The concentration of **Ir-1** and **Ir-2** in the medium was measured using UV-visible spectrophotometer.

4.6. Cell cytotoxicity assay

The cytotoxic activity of the complexes and liposomes against the selected cancer cell lines was assayed by MTT method [59]. Cancer cells suspension were seeded in 96-well plates (approximately 1×10^4 cells per well) and grown further to appropriate density in a 37 ^{o}C, 5% CO_2 incubator. All compounds and liposomes to be tested were dissolved in DMSO and the final concentration range after addition to the wells ranged from 1-100 μM. At the same time, an equal volume of pure DMSO solution was added to the corresponding plate well as a control group. When the 96-well plate was incubated for 48 h, the liquid in the wells was removed and replaced with 90 μL of medium and 10 μL of MTT dye solution (20 μL, 5mg·mL^{-1}). The dye-filled 96-well plate was placed in a 37 °C, 5% CO_2 incubator for 4 h. After the incubation, each well will be added with 100 μL of DMSO solution to dissolve the formazan produced by MTT. The absorbance of each well was measured by a microplate reader at a wavelength of 490 nm. The IC_{50} value was determined by plotting the logarithm of the concentration versus the percentage of viable cells and the results of the SPSS software analysis. To ensure the accuracy of the data, each set of experiments will be repeated at least three times and the average will be calculated.

4.7. Apoptosis assay by flow cytometry

When B16 cells are tightly attached in a 6-well plate and grown at a higher density, the medium removed from the wells will be replaced with medium containing **Ir-1** or **Ir-2** and different concentrations of **Ir-1-Lipo** or **Ir- 2-Lipo** incubation for 24 h. After washing the cells in the wells three times with cold phosphate buffer PBS, collection was performed simultaneously with trypsin-EDTA. The supernatant was removed and washed in a desktop low temperature centrifuge, stained in a flow tube with PBS solution containing 500 mg / mL of pyridine pyridinium (PI) and 1 mg / mL annexin V-FITC in a dark low temperature environment. Fluorescence emission of the dye-treated cells was measured at 530 nm by excitation at 488 nm using a FACS Calibur flow cytometer (Beckman Dickinson & Co., Franklin Lakes, NJ). It is worth noting that sufficient number of cells is a guarantee of the accuracy of sample data.

4.8. Reactive oxygen species (ROS) detection

The specific fluorescent probe 2′,7′-dichlorodihydrofluorescein diacetate (DCHF-DA, 10 μM) was used to investigate changes in intracellular ROS levels induced by liposomes. The cells were seeded at a density of 1.5×10^5 per well in a 12-well plate and incubated overnight. The liquid in the wells was removed while replacing the medium containing the corresponding concentrations of these liposomes and incubated for 24 h. After treatment with these liposomes, the cells in the wells were washed three times with PBS and incubated with fluorescent probes. After

incubation for 30 min, the liquid in the wells was removed and the excess dye was washed with PBS solution. The cells in the 12-well plate were imaged by ImageXpress Micro XLS system (MD Company, US), and the DCF fluorescence intensity was calculated and analyzed.

4.9. Mitochondrial membrane potential assay

Widely used mitochondrial membrane potential fluorescent probe JC-1 for membrane potential detection of B16 cells. Cells (about 2×10^6) were seeded in 12-well plates, followed by treatment with corresponding concentrations of liposomes for 24 h. Then remove the medium from the 12 wells, wash the cells several times with PBS, and stain with the fluorescent probe JC-1. After incubation for 20 min at room temperature, PBS washed the excess dye in the wells and image the cells using ImageXpress Micro XLS system (MD Company, US).

4.10. Cell cycle arrest studied

B16 cell suspension was seeded in a 6-well plate at a density of 5×10^5 per well and incubated until tightly attached. After the incubation, discard the liquid in the wells and re-add the medium containing the corresponding concentration of liposomes and incubate for 24 h. After the end of the liposome treatment, the cells obtained by trypsin digestion were washed with PBS on a centrifuge. After being fixed overnight with 75% alcohol, 20 μL of RNAse (0.2 mg / mL) and 20 μL of propidium iodide (0.02 mg / mL) were thoroughly mixed with the cells and incubated for 30 min at

room temperature. The number of cells in the sample is also an important factor influencing the data, while the samples were analyzed using a FACS Calibur flow cytometer. Therefore, we always ensure that the number of cells per sample analyzed is not less than 10,000 [60].

4.11. Western blot analysis

When the B16 cells in the 6-well plate were grown in an excellent state, the old medium was discarded and the medium containing **Ir-1**, **Ir-2** and different concentrations of **Ir-1-Lipo** or **Ir-2-Lipo** was separately added. B16 cells after 24 h of incubation were placed in ice cubes, protein suspensions were quickly obtained by cell lysis buffer and then placed in a high speed refrigerated centrifuge for 15 min. After obtaining the supernatant, the protein concentration of each sample obtained by the treatment is determined by the BCA detection method. The obtained protein samples were separately electrophoresed in each lane of sodium dodecyl sulfate-polyacrylamide gel by equal volume addition of a microinjector. The isolated gel was transferred to a PVDF membrane and then blocked with TBST buffer containing 5% skim milk powder for 4 h. After washing the skim milk powder with PBST buffer, the PVDF membrane containing the protein molecule was incubated with the specific protein primary antibody at 4 ^{o}C overnight. After washing four times with PBST buffer on a shaker, the labeled secondary antibody was incubated with the PVDF membrane bound to the primary antibody for 1 h. Finally, we showed the blot according to the Amersham ECL Plus Western blot detection reagent. To assess the

presence of comparable amount of proteins in each lane, the membranes were stripped finally to detect the β-actin.

4.12. Comet assay

DNA damage was investigated by means of comet assay. B16 cells in culture medium were incubated with 5 μM of the complexes and liposomes at 37 °C for 24 h. The cells were harvested by a trypsinization process at 24 h. A total of 100 μL of 0.5% normal agarose in PBS was dropped gently onto a fully frosted microslide, covered immediately with a coverslip, and then placed at 4 °C for 10 min. The coverslip was removed after the gel has been fixed. 50 μL of the cell suspension (200 cells /μL) was mixed with 50 μL of 1% low melting agarose preserved at 37 °C. A total of 100 μL of this mixture was applied quickly on top of the gel, coated over the microslide, covered immediately with a coverslip, and then placed at 4 °C for 10 min. The coverslip was again removed after the gel has been fixed. A third coating of 50 μL of 0.5% low melting agarose was placed on the gel and allowed to place at 4 °C for 15 min. After solidification of the agarose, the coverslips were removed, and the slides were immersed in an ice-cold lysis solution (2.5 M NaCl, 100 mM EDTA, 10 mM Tris, 90 mM sodium sarcosinate, NaOH, pH 10, 1% Triton X-100 and 10% DMSO) and placed in a refrigerator at 4 °C for 2 h. All of the above operations were performed under low lighting conditions to avoid additional DNA damage. After the removal of the lysis solution, the slides were placed horizontally in an electrophoresis chamber. The reservoirs were filled with an electrophoresis buffer (300 mM NaOH, 1.2 mM

EDTA) until the slides were just immersed in the buffer solution, and the DNA was allowed to unwind for 30 min in the electrophoresis solution. Then the electrophoresis was carried out at 25 V and 300 mA for 20 min. After electrophoresis, the slides were removed, and washed thrice in a neutralization buffer (400 mM Tris, HCl, pH 7.5). Nuclear DNA was stained with 20 μL of EtBr (20 μg/mL) in the dark for 20 min. The slides were washed in chilled distilled water for 10 min to neutralize the excess alkali, air-dried and scored for comets by fluorescence microscopy. A total of 10 comets on each gel were scored.

4.13. Matrigel invasion assay

A BD Matrigel invasion chamber was used to investigate cell invasion according to the manufacturer's instructions. B16 cells (4×10^4) in serum free medium containing different concentrations of the complexes and liposomes were seeded into the top chamber of the two-chamber Matrigel system. RPMI 1640 medium (20% FBS) was added into the lower chamber. The cells were allowed to invade for 24 h. After incubation, non-invading cells were removed from the upper surface and cells on the lower surface were fixed with 4% paraformaldehyde and stained with 0.1% crystal violet. The membranes were photographed and the invading cells were counted under a light microscope. The mean values from three independent assays were calculated.

4.14. Measurement of Intracellular Ca^{2+} level

B16 cells were treated with different concentrations of the complexes and

liposomes for 24 h, the cells were incubated with Fluo-3AM for 30 min at 37 ^{o}C in the dark, and washed with PBS three times, then incubated an additional 20 min with PBS at 37 ^{o}C to ensure that Fluo-3AM has been completely transformed into Fluo-3, which can specifically bind to Ca^{2+} and has a strong fluorescence with an excitation wavelength of 488 nm. The cell nuclei were stained with DAPI at 37 ^{o}C. Finally, ImageXpress Micro XLS system was used to observe fluorescence, and Multi Wavelength Cell Scoring module was used to analyze the data. The integrated intensity/cell which represented the fluorescence intensity of each cell was used to measure the levels of Ca^{2+}. The fluorescence intensity of each cell was calculated as the total fluorescence intensity divided by the number of cells.

4.15. Release of cytochrome c studies

B16 cells were seeded in a 12-well plate and incubated overnight. Then cells were treated with different concentrations of the complexes and liposomes for 24 h. Subsequently, the cells were fixed with ice-cold immunol staining fix solution for 30 min at room temperature. After blocking cells with immunol staining blocking buffer for 1 h, the cells were treated with the primary antibody against cytochrome c (1:50 dilution) overnight at 4 ^{o}C. Next, the plate was washed with immunol staining wash buffer three times and probed with Alexa Fluor 488-Labeled Goat Anti-Mouse IgG (1:500 dilution) in the dark for 1 h at room temperature. Finally, the cells were washed with immunol staining wash buffer three times and the cell nuclei were stained with DAPI. The images were obtained using ImageXpress Micro XLS system,

and Multi Wavelength Cell Scoring module was used to analyze the data. The integrated intensity/cell which represents the fluorescence intensity of each cell was used to measure the release of cyto-c. The fluorescence intensity of each cell was calculated as the total fluorescence intensity divided by the number of cells.

4.16. Targeting microtubules studies

B16 cells were grown at a density of 10^6 cells /mL and incubated in the presence of the complexes and liposomes for 24 h. Subsequently cells were washed twice by PBS, fixed with 2% paraformaldehyde, and incubated with immunostaining blocking solution for 1 h. Cells were then mildly washed with immunostaining wash solution. Subsequently, cells were incubated with antirabbit monoclonal anti-α-tubulin antibody (1:100 dilutions) for 24h at 4 ^oC, followed by anti-rabbit FITC conjugated IgG antibody (1:500 dilutions) and DAPI (10 μg/mL). After incubation, cells were washed with PBS and viewed under a fluorescence microscope.

*4.17. Antitumor efficacy of **Ir-1** and **Ir-1-Lipo** in xenograft tumor mice*

Mice with human tumor xenografts (HOS) were provided by the Laboratory Animal Center of Sun Yat-Sen University. **Ir-1** (6.0 mg/kg) and different doses of 4.8 and 9.6 mg/kg of **Ir-1-Lipo** were injected intraperitoneally into mice of different group (each group contained 6 mice) once a day for seven consecutive days beginning 24 h after inoculation. This dose was the maximum tolerated dose based on our preliminary studies. Control mice were injected with the vehicle. Compounds were

administered by exact body weight, with the injection volume being not more than 0.2 mL. The weights of the animals were recorded every day. All animals were sacrificed on the eighth days after tumor inoculation, and the tumors were excised and weighed. The inhibition rate was calculated as follow:

$$[(C - T)/C] \times 100\%$$

T is the average tumor weight of the treated group and C is the average tumor weight of the negative control group [61].

4.18. Data analysis

All data was expressed as means ± SD. Statistical significance was evaluated by a t-test. Differences were considered to be significant when a $*P$ value is less than 0.05.

Acknowledgements

This work was supported by the National Nature Science Foundation of China (No 21877018) and the Natural Science Foundation of Guangdong Province (No 2016A030313728).

Live subject statement

All animal procedures were performed in accordance with the Guidelines for Care and Use of Laboratory Animals of Guangdong Pharmaceutical University and Experiments were approved by the Animal Ethics Committee of Guangdong Pharmaceutical University.

References

[1] M. Kanapathipillai, A. Brock, D.E. Ingber, *Adv. Drug Deliv. Rev.* 107 (2014) 79-80.

[2] I.J. Fidler, *Semin. Cancer Biol*. 12 (2002) 89-96.

[3] A.M. Meredith, C.R. Dass, *J. Pharm. Pharmacol*. 268 (2016) 729-741.

[4] Z. Liu, A. Habtemariam, A.M. Pizarro, S.A. Fletcher, A. Kisova, O. Vrana, L. Salassa, P.C.A. Bruijnincx, G.J. Clarkson, V. Brabec, P.J. Sadler, *J. Med. Chem*. 54 (2011) 3011-3026.

[5] A.M. Florea, D. Büsselberg, *Cancers*, 3 (2011) 1351-1371.

[6] A. Rajeswaran, A. Trojan, B. Burnand, M. Giannelli, *Lung Cancer*. 59 (2008) 1-11.

[7] Z. Liu, I. Romero-Canelon, B. Qamar, J.M. Hearn, A. Habtemariam, N.P.E. Barry, A.M. Pizarro, G.J. Clarkson, P.J. Sadler, *Angew. Chem. Int. Ed.* 53 (2014) 3941-3946.

[8] Z. Liu, P.J. Sadler, *Accounts Chem. Res.* 47 (2014) 1174-1185.

[9] C.H. Leung, H.J. Zhong, D.S.H. Chan, D.L. Ma, *Coord. Chem. Rev.* 257 (2013) 1764-1776.

[10] K. Henze, W. Martin, *Nature*. 426 (2002) 127-128.

[11] H.M. McBride, M. Neuspiel, S. Wasiak, *Curr. Biol*. 16 (2006) 551-560.

[12] R.J. Youle, D.P. Narendra, *Nat. Rev. Mol. Cell Biol*. 12 (2011) 9-14.

[13] N. Mosallaei, A. Mahmoudi, H. Ghandehari, V.K. Yellepeddi, M.R. Jaafari, B.

Malaekeh-Nikouei, *Eur. J. Pharm. Biopharm.* 104 (2016) 42-50.

[14] H. Zhang, J. Wang, W. Mao, J. Huang, X. Wu, Y. Shen, M. Sui, *J. Control Release*. 166 (2013) 147-158.

[15] T.M. Basel, S. Balivada, B.T. Shrestha, G.M. Seo, M.M. Pyle, M. Tamura, S.H. Bossmann, D.L. Troyer, *Small*, 8 (2012) 913-920.

[16] V. Bala, S. Rao, P. Li, S. Wang, C.A. Prestidge, *Mol. Pharm*. 13 (2016) 287-294.

[17] H. Zhao, B. Rubio, P. Sapra, D. Wu, P. Reddy, P. Sai, A. Martinez, Y. Gao, Y. Lozanquiez, C. Longley, L.M. Greenberger, I.D. Horak, *Bioconjug. Chem.* 19 (2008) 849-859.

[18] X. Cheng, N. Qiu, J. Yang, H. Liu, J. Wen, W. Wang, Z. Wang, L. Chen, *J. Pharm. Sci*. 104 (2015) 3934-3942.

[19] J.A. Zhang, T. Xuan, M. Parmar, L. Ma, S. Ugwu, S. Ali, I. Ahmad, *Int. J. Pharm*. 270 (2004) 93-107.

[20] Q. Xie, W. Deng, X. Yuan, H. Wang, Z. Ma, B. Wu, X. Zhang, *Eur. J. Pharm. Biopharm.* 122 (2017) 87-95.

[21] A. Mohan, S. Narayanan, G. Balasubramanian, S. Sethuraman, U.M. Krishnan, *Eur. J. Pharm. Biopharm.* 99 (2016) 73-83.

[22] T.H. Tran, J.Y. Choi, T. Ramasamy, D. H. Truong, C.N. Nguyen, H.G. Choi, C.S. Yong, J.O. Kim, *Carbohydr. Polym.* 114 (2014) 407-415.

[23] H. Kouchakzadeh, S.A. Shojaosadati, A. Maghsoudi, E.V. Farahani, *AAPS Pharm. Sci. Tech*. 11 (2010) 1206-1211.

[24] M. Reich, P.F. Van Swieten, V. Sommandas, M. Kraus, R. Fischer, E. Weber, H.

Kalbacher, H.S. Overkleeft, C. Driessen, *J. Leukocyte. Biol*. 81 (2007) 990-1001.

[25] M.E. Guicciardi, M. Leist, G.J. Gores, *Oncogene*, 23 (2004) 2881-2890.

[26] M. Ghosh, F. Carlsson, A. Laskar, X. Yuan, W. Li, *FEBS Lett*. 585 (2011) 623-629.

[27] Y. Chang, Y. Li, N. Ye, X. Guo, Z. Li, G. Sun, Y. Sun, *Apoptosis*, 21 (2016) 977-996.

[28] Q.Y. Yi, D. Wan, B. Tang, Y.J. Wang, W.Y. Zhang, M. He, Y.J. Liu, *Eur. J. Med. Chem*. 145 (2018) 339-349.

[29] B. Tang, D. Wan, Y.J. Wang, Q.Y. Yi, B.H. Guo, Y.J. Liu, *Eur. J. Med. Chem*. 145 (2018) 302-314.

[30] W.Y. Zhang, Q.Y. Yi, Y.J. Wang, F. Du, M. He, B. Tang, D. Wan, Y.J. Liu, H.L. Huang, *Eur. J. Med. Chem*. 151 (2018) 568-584.

[31] A.T. Hoye, J.E. Davoren, P. Wipf, M.P. Fink, V.E. Kagan, *Acc. Chem. Res*. 41 (2008) 87-97.

[32] L.M. Chen, F. Peng, G.D. Li, X.M. Jie, K.R. Cai, C. Cai, Y. Zhong, H. Zeng, W. Li, Z. Zhang, J.C. Chen, *J. Inorg. Biochem.* 156 (2016) 64-74.

[33] M. Reers, S.T. Smiley, C. Mottola-Hartshorn, A. Chen, M. Lin, L.B. Chen, *Methods Enzymol*. 260 (1995) 406-417.

[34] S. Salvioli, R. Maseroli, T.L. Pazienza, V. Bobyleva, A. Cossarizza, *Biochemistry.* 63 (1998) 235-238.

[35] L.B. Sullivan, N.S. Chandel, *Cancer & Metabolism.* 2 (2014) 1-12.

[36] E. Panieri, M.M. Santoro, *Cell Death Dis*. 7 (2016) 2253-2265.

[37] E. Carafoli, *Proc. Natl. Acad. Sci. USA*. 99 (2002) 1115-1122.

[38] J. Li, P. Wang, S. Yu, Z. Zheng, X. Xu, *Mol. Vis*. 18 (2012) 2371-2379.

[39] D. Penzo, V. Petronilli, A. Angelin, C. Cusan, R. Colonna, L. Scorrano, P. Bernardi, *J. Biol. Chem.* 279 (2004) 25219-25225.

[40] S.F. An, Y. Gao, Y.H. Huang, X.Q. Jiang, K. Ma, J.Q. Ling, *Int. J Mol. Med*. 36 (2015) 215-221.

[41] J. Yang, X. Liu, K. Bhalla, C.N. Kim, A.M. Ibrado, J. Cai, T.I. Peng, D.P. Jones, X. Wang, *Science,* 275 (1997) 1129-1132.

[42] R.M. Kluck, E. Bossy-Wetzel, D.R. Green, D.D. Newmeyer, *Science,* 275 (1997) 1132-1136.

[43] G.P. Gupta, J. Massagué, *Cell.* 127 (2006) 679-695.

[44] S. Tsuda, M. Naonari, U. Shunji, S. Nobuyuki, F.S. Yu, *Toxicol. Sci*. 54 (2000) 104-109.

[45] A.A. Goyeneche, R.W. Caron, C.M. Telleria, *Clinical Cancer Res.* 13 (2007) 3370-3379.

[46] M.B. Kastan, J. Bartek, *Nature*, 432 (2004) 316-323.

[47] M.A. Jordan, L. Wilson, *Nat. Rev. Cancer,* 4 (2004) 253-265.

[48] V.J. Prasad, L. Christoph, *Nat. Rev. Cancer,* 1 (2001) 109-117.

[49] N.D. Lakin, S.P. Jackson, *Oncogene*, 18 (1999) 7644-7655.

[50] K.M. Murphy, V. Ranganathan, M. Farnsworth, L.M. Kavallaris, R.B. Lock, *Cell Death Differ*. 7 (2000) 102-111.

[51] A. Tyagi, R.P. Singh, C. Agarwal, R. Agarwal, *Carcinogenesis*, 27 (2006)

2269-2280.

[52] P.J. Duriez, G.M. Shah, *Cell Biol*. 75 (1997) 337-349.

[53] D.R. Green, G.I. Evan, *Cancer Cell*. 1 (2002) 19-30.

[54] K. Yip, J. Reed, *Oncogene*, 27 (2008) 6398-6406.

[55] S. Sprouse, K.A. King, P.J. Spellane, R.J. Watts, *J. Am. Chem. Soc.* 106 (1984) 6647-6653.

[56] Z.B. Cai, L.F. Liu, Y.Q. Hong, M. Zhou, *J. Coord. Chem.* 66 (2013) 2388-2397.

[57] Q.F. Guo, S.H. Liu, Q.H. Liu, H.H. Xu, J.H. Zhao, H.F. Wu, X.Y. Li, J.W. Wang, *J. Coord. Chem*. 65 (2012) 1781-1791.

[58] F.D. Szoka, D. Papahadjopoulos, *Proc.Natl. Acad. Sci.* USA. 75 (1978) 4194-4198.

[59] T. Mosmann, *J. Immunol. Methods*, 65 (1983) 55-63.

[60] K.K. Lo, T.K. Lee, J.S. Lau, W.L. Poon, S.H. Cheng. *Inorg. Chem.* 47 (2008) 200-208.

[61] R.H. Cao, Q. Chen, X.R. Hou, H.S. Chen, H.J. Guan, Y. Ma, W.L. Peng, A.L. Xu, *Bioorg. Med. Chem.* 12 (2004) 4613-4623.

Captions for Schemes and Figures

Table 1 IC_{50} values of the complex and liposomes toward selected cancer cell lines

Scheme 1 Structures of complexes **Ir-1** and **Ir-2**

Fig. 1 Percentage of release of **Ir-1** and **Ir-2** from **Ir-1-Lipo** and **Ir-2-Lipo**

Fig. 2 Location assay of **Ir-1-Lipo** (5.0 μM) and **Ir-2-Lipo** (10.0 μM) in the lysosomes after B16 cells were exposed to the liposomes for 0.5 h.

Fig. 3 Location assay of **Ir-1-Lipo** (5.0 μM) and **Ir-2-Lipo** (10.0 μM) in the mitochondria after B16 cells were treated with the liposomes for 1 h.

Fig. 4 (A) Intracellular Ca^{2+} levels were assayed after B16 cells were exposed to **Ir-1-Lipo** (5.0 μM) and **Ir-2-Lipo** (10.0 μM) for 24 h. (B) The integrated fluorescent intensity/cell was determined after B16 cells were treated with **Ir-1** (5.0 μM), **Ir-2** (10.0 μM) and different concentration of **Ir-1-Lipo** and **Ir-2-Lipo** for 24 h. $*P < 0.05$ represents significant differences compared with control.

Fig. 5 (A) The release of cyt-c was examined after B16 cells were exposed to **Ir-1-Lipo** (5.0 μM) and **Ir-2-Lipo** (10.0 μM) for 24 h. (B) The integrated fluorescent intensity/cell was determined after B16 cells were incubated with **Ir-1** (5.0 μM), **Ir-2** (10.0 μM) and different concentration of **Ir-1-Lipo** and **Ir-2-Lipo** for 24 h. $*P < 0.05$ represents significant differences compared with control.

Fig. 6 Apoptosis assays after B16 cells (a) were treated with **Ir-1** (b, 5.0 μM), **Ir-2** (e,

10.0 μM) and 2.5 and 5.0 μM of **Ir-1-Lipo** (c and d) and 5.0 and 10.0 μM of **Ir-2-Lipo** (f and g) for 24 h.

Fig. 7 The expression of CDK2 and Cyclin A2 proteins of B16 cells (a) induced by (A): **Ir-1** (b, 5.0 μM), 2.5 and 5.0 μM of **Ir-1-Lipo** (c and d); (B) **Ir-2** (b, 10.0 μM) and 5.0 and 10.0 μM of **Ir-2-Lipo** (c and d) for 24 h.

Fig. 8 Assays of microtubules networks of B16 cells (a) induced by 2.5 and 5.0 μM of **Ir-1-Lipo** (b and c), 5.0 and 10.0 μM of **Ir-2-Lipo** (e and f) for 24 h.

Fig. 9 The expression of caspase-3, PARP and Bcl-2 family proteins after B16 cells were treated with **Ir-1**, **Ir-1-Lipo**, **Ir-2** and **Ir-2-Lipo** for 24 h.

Fig. 10 The in vivo antitumor activity of **Ir-1-Lipo** in B16 xenograft model. (A) Tumor volume growth trend of control group, 6.0 mg/kg of **Ir-1**, 4.8 mg/kg and 9.6 mg/kg of **Ir-1-Lipo** groups. Tumor volumes were tracked by the mean tumor volume (cm^3) ± SD (n = 6) and calculated as relative tumor growth rate [T/C%] values. (B) Photographs of tumor from treatment groups and vehicle group. (C) Tumor weight (mean ± SD) mg after the tumor was treated with **Ir-1** or **Ir-1-Lipo** for 7 days. (D) Inhibiting percentage of tumor growth induced by 6.0 mg/kg **Ir-1** and different concentrations of **Ir-1-Lipo**. *P < 0.05 represents significant differences compared with control.

Fig. 11 The mechanism of **Ir-1-Lipo** and **Ir-2-Lipo** inducing apoptosis in B16 cells.

Table 1 IC_{50} values of the complex and liposomes toward selected cancer cell lines

Complex	B16	HeLa	SGC-7901	MCF-7	A549	BEL-7402	LO2
Ir-1	> 200	> 200	> 200	> 200	> 200	> 200	> 200
Ir-1-Lipo	5.2 ± 0.8	9.5 ± 0.9	8.7 ± 0.3	13.9 ± 1.6	10.3 ± 0.7	12.0 ± 2.4	15.0 ± 1.3
Ir-2	> 200	> 200	> 200	> 200	> 200	> 200	> 200
Ir-2-Lipo	10.8 ± 1.5	6.2 ± 0.4	8.0 ± 1.2	21.0 ± 1.6	10.8 ± 0.8	11.3 ± 0.5	22.3 ± 1.8

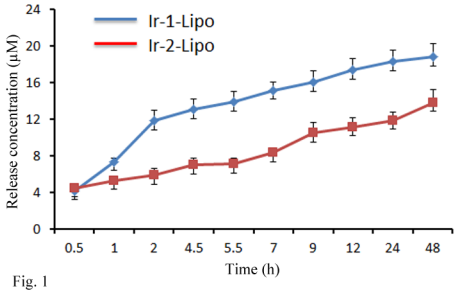

Fig. 1

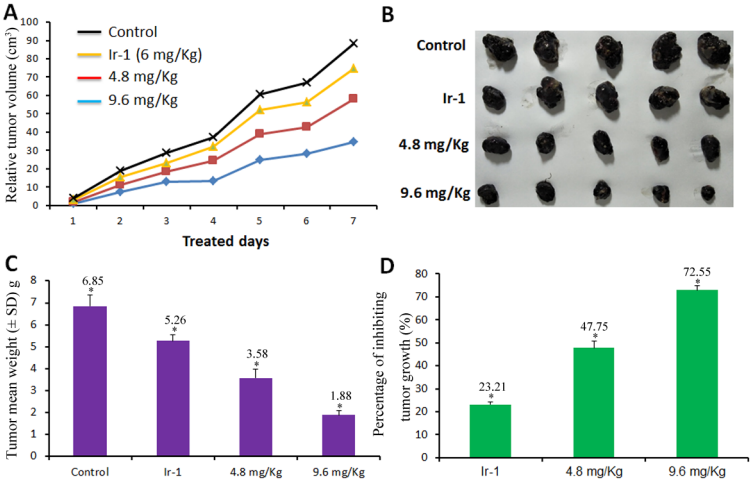

Fig. 10

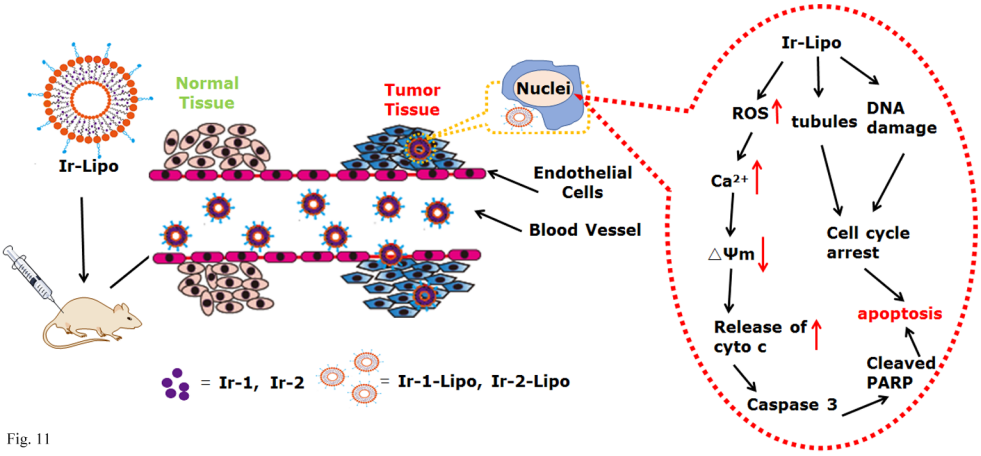

Fig. 11

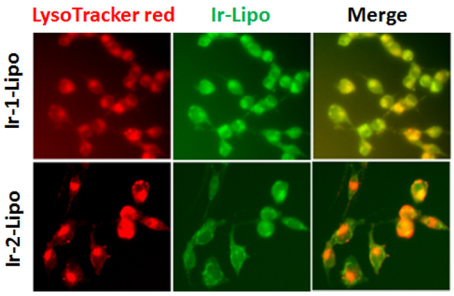

Fig. 2

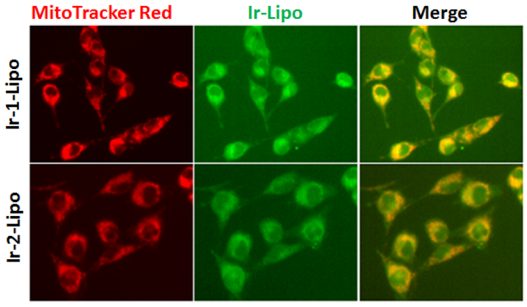

Fig. 3

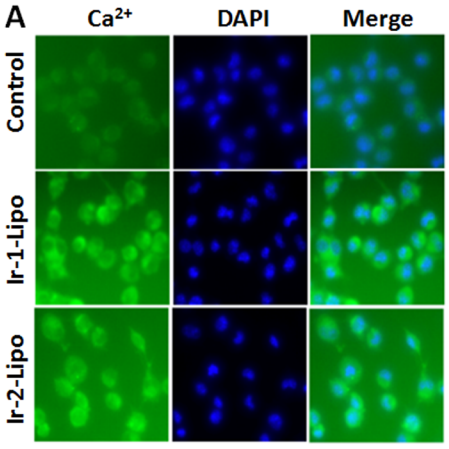

Fig. 4A

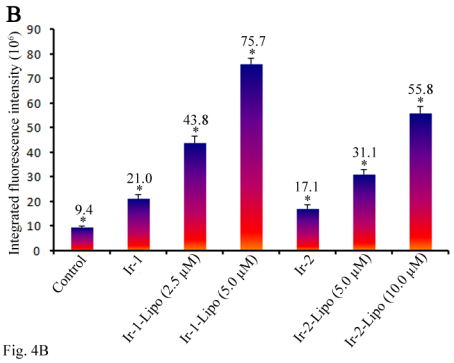

Fig. 4B

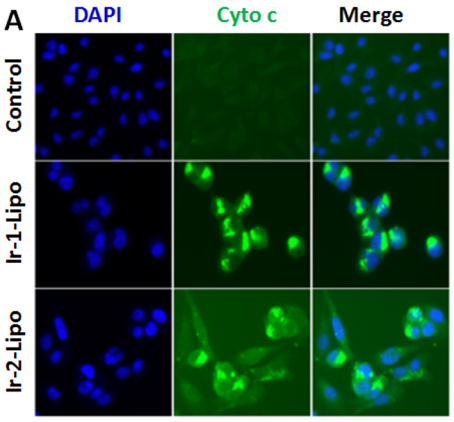

Fig. 5A

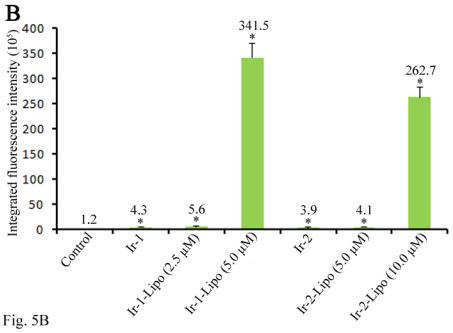

Fig. 5B

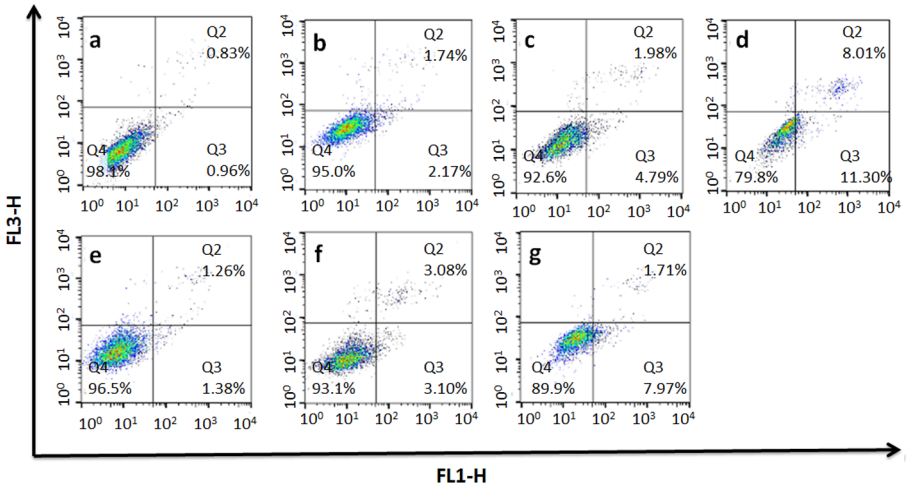

Fig. 6

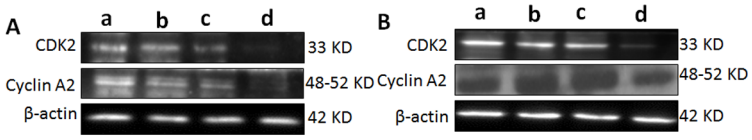

Fig. 7

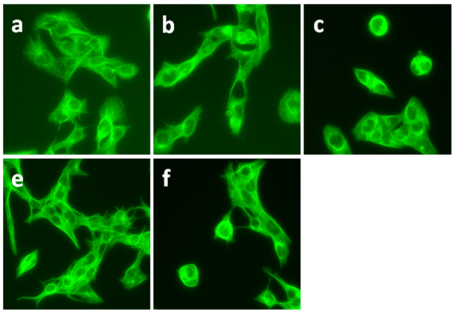

Fig. 8

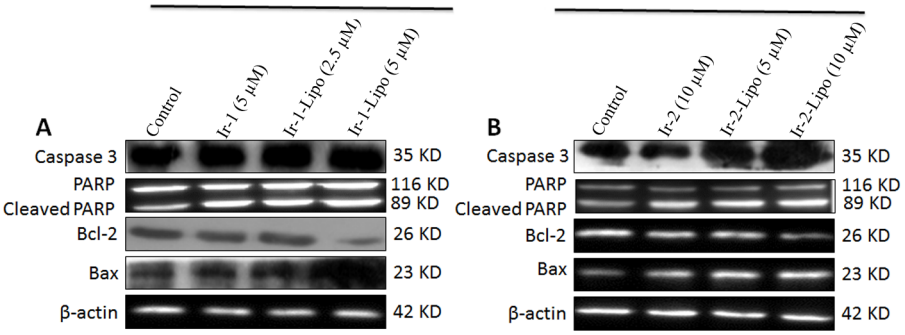

Fig. 9

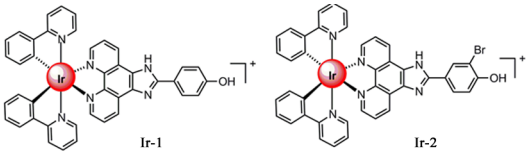

Ir-1

Ir-2

Scheme 1

Highlights

- Two iridium(III) complexes **Ir-1** and **Ir-2** and their liposomes **Ir-1-Lipo** and **Ir-2-Lipo** were synthesized and characterized.
- The cytotoxicity in vitro or in vivo of the complexes and liposomes was investigated.
- The apoptosis and cell cycle distribution were assayed by flow cytometry
- ROS and mitochondrial membrane potential were studied under fluorescence microscope.
- The expression of Bcl-2 family proteins was assayed by western blot analysis.